

A Comparative Study of Adaptive Interlimb Coordination Mechanisms for Self-Organized Robot Locomotion

Tao Sun^{1,2}, Xiaofeng Xiong², Zhendong Dai¹, Dai Owaki³, and Poramate Manoonpong^{1,2,*}

¹*Institute of Bio-inspired Structure and Surface Engineering, College of Mechanical and Electrical Engineering, Nanjing University of Aeronautics and Astronautics, Nanjing, China*

²*Embodied AI & Neurobotics Lab, SDU Biorobotics, Mærsk Mc-Kinney Møller Institute, University of Southern Denmark, Odense M, Denmark*

³*Department of Robotics, Graduate School of Engineering, Tohoku University, Japan*

Correspondence*:
Poramate Manoonpong
poma@mmmi.sdu.dk

2 ABSTRACT

3

4 Walking animals demonstrate impressive self-organized locomotion and adaptation to body
5 property changes by skillfully manipulating their complicated and redundant musculoskeletal
6 systems. Adaptive interlimb coordination plays a crucial role in this achievement. It has been
7 identified that interlimb coordination is generated through dynamical interactions between the
8 neural system, musculoskeletal system, and environment. Based on this principle, two classical
9 interlimb coordination mechanisms (continuous phase modulation and phase resetting) have been
10 proposed independently. These mechanisms use decoupled central pattern generators (CPGs)
11 with sensory feedback, such as ground reaction forces (GRFs), to generate robot locomotion
12 autonomously without predefining it (i.e., self-organized locomotion). A comparative study was
13 conducted on the two mechanisms under decoupled CPG-based control implemented on a
14 quadruped robot in simulation. Their characteristics were compared by observing their CPG
15 phase convergence processes at different control parameter values. Additionally, the mechanisms
16 were investigated when the robot faced various unexpected situations, such as noisy feedback,
17 leg motor damage, and carrying a load. The comparative study reveals that the phase modulation
18 and resetting mechanisms demonstrate satisfactory performance when they are subjected to
19 symmetric and asymmetric GRF distributions, respectively. This work also suggests a strategy for
20 the appropriate selection of adaptive interlimb coordination mechanisms under different conditions
21 and for the optimal setting of their control parameter values to enhance their control performance.

22 **Keywords:** Adaptive interlimb coordination, phase resetting, phase modulation, decoupled CPGs, sensory feedback, self-organized
23 locomotion.

1 INTRODUCTION

24 Walking animals demonstrate impressive self-organized locomotion and adaptation to body property
25 changes by skillfully manipulating their complicated and redundant musculoskeletal systems (Taga et al.,
26 1991; Dickinson et al., 2000; Grabowska et al., 2012; Der and Martius, 2012). Many studies have clarified
27 that adaptive interlimb coordination plays a crucial role in this achievement (Aoi et al., 2017; Mantziaris
28 et al., 2017). Investigations of various aspects of adaptive interlimb coordination mechanisms have attracted
29 significant attention in various research fields.

30 To demonstrate these mechanisms, biologists have proposed some neurological principles, such as
31 central pattern generators (CPGs) (Marder and Bucher, 2001), reflex chains (Grillner, 1975), and sensory
32 feedback (Grillner, 2003; Rossignol et al., 2006), through biological experiments. In addition, roboticists
33 have developed many bio-inspired neural control schemes for legged robots to emulate animal-like self-
34 organized locomotion (Kimura et al., 2007; Owaki et al., 2013; Barikhan et al., 2014; Ambe et al., 2018;
35 Fukui et al., 2019; Miguel-Blanco and Manoonpong, 2020). To realize self-organized locomotion and
36 adaptation on artificial legged systems, many adaptive robot control schemes based on distributed abstract
37 CPGs incorporating ground reaction force (GRF) feedback have been proposed (Kimura et al., 2007; Owaki
38 et al., 2013; Barikhan et al., 2014; Ambe et al., 2018; Fukui et al., 2019). Specifically, the GRF feedback is
39 exploited to modulate the phase relationships of the CPGs under two main strategies: (continuous) phase
40 modulation (PM) and (discrete) phase resetting (PR).

41 PM typically uses continuous GRFs to modulate CPG phases continuously (Kimura et al., 2007;
42 Owaki et al., 2013; Barikhan et al., 2014; Owaki et al., 2017; Fukuhara et al., 2018; Miguel-Blanco
43 and Manoonpong, 2020). In contrast, the PR uses discrete GRFs to reset the CPG phases intermittently
44 (Tsujita et al., 2001; Aoi and Tsuchiya, 2007; Nomura et al., 2009; Aoi et al., 2010, 2012; Ambe et al.,
45 2018). While both mechanisms have proved their effectiveness in their own right and have been widely
46 used in various fashions, they have not been systematically analyzed and compared to identify their
47 characteristics in detail. For instance, how the control parameter values of the mechanisms influence the
48 phase convergence process and whether the mechanisms show different performances in different situations.
49 It is necessary to consider in which situations the PM (PR) works better.

50 From this point of view, a comparative study of the PM and PR for self-organized locomotion was
51 conducted. They were used to modulate four decoupled neural SO (2)-based CPGs¹ (Pasemann et al., 2003)
52 relying on local GRF information. The modulated CPGs, acting as an adaptive neural controller, were
53 implemented on a quadruped robot in simulation, as shown in Figures 1 (A) and (B). The CPG outputs were
54 utilized to drive the robot joint movements such that the robot could autonomously perform self-organized
55 locomotion, as shown in Figure 1 (C). The study focused on: 1) the parameter characteristics of the PM and
56 PR and 2) their adaptations to unexpected robot situations (e.g., noisy feedback, leg motor damage, and
57 carrying a load). The validation of the study was quantified by three metrics including: phase convergence
58 time, phase deviation, and cost of transport (COT). Consequently, this work provides suggestions on how
59 to choose adaptive interlimb coordination mechanisms properly in different situations and set their control
60 parameter values optimally to enhance their control performance.

61 The rest of this article is structured as follows. Details of the materials and methods are provided in
62 Section 2. The experimental results are presented in Section 3. A discussion of the experimental results and
63 the conclusions are provided in Section 4.

¹ Note that an SO (2)-based CPG is a special type of 2-neuron network where the weight matrix of the network is an element in the special orthogonal group SO(2).

2 MATERIALS AND METHODS

64 In this section, the adaptive neural controller for studying the PM and PR is elucidated. It is composed of
 65 four identical and decoupled neural SO (2)-based CPGs (Pasemann et al., 2003; Sun et al., 2018) modulated
 66 by the PM or PR. Subsequently, a simulation environment with a quadruped robot (called "Lilibot") is
 67 introduced. It is an experimental platform for assessing the PM and PR by implementing the adaptive neural
 68 controller on the robot to generate self-organized locomotion. In addition, certain variables and metrics for
 69 analyzing and assessing the CPG phase convergence and self-organized locomotion are introduced.

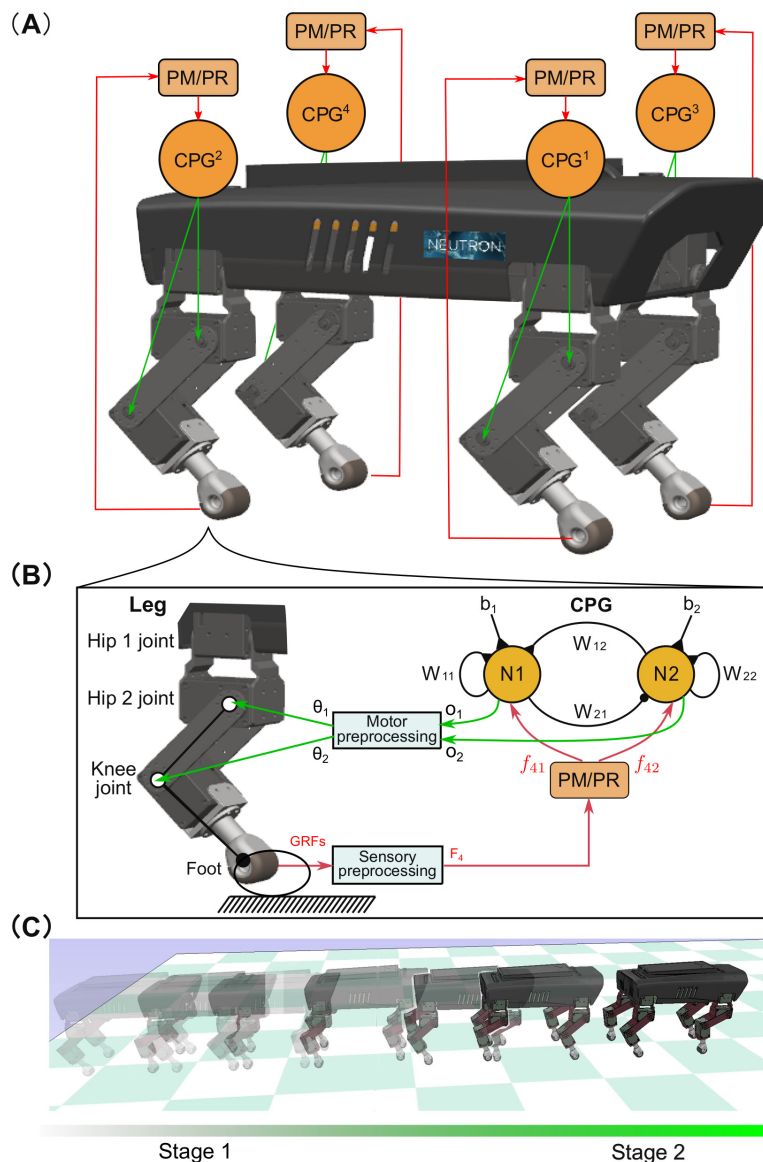


Figure 1. (A) Four identical and decoupled neural SO (2)-based CPGs modulated by the PM or PR relying on the sensory feedback (i.e., GRFs). They are used to control a quadruped robot. (B) Each CPG is composed of two mutually connected neurons. It outputs two synchronized signals ($o_{1,2}$). The signals are linearly re-scaled as motor commands ($\theta_{1,2}$) for controlling the hip 2 and knee joints of a leg through the motor preprocessing unit. For simplicity, here the hip 1 joint is kept fixed and set to a certain position. (C) The quadruped was demonstrated under the self-organized locomotion generation process. The process was divided into two stages: transition (Stage 1) and formation (Stage 2).

70 2.1 Adaptive neural controller

71 The adaptive neural controller integrates the four CPGs with either PM or PR. The controller was
 72 proposed for easily demonstrating the PM and PR in an integrative manner. The PM and PR have numerous
 73 forms that comply with different CPG models and robots (Kimura et al., 2007; Owaki et al., 2013; Barikhan
 74 et al., 2014; Sun et al., 2020). To compare the PM and PR conveniently and consistently, four neural SO (2)
 75 oscillators are used as four decoupled CPGs. The SO (2)-based CPG has a simple neural network topology
 76 with analyzable neural dynamics (Pasemann et al., 2003). Thus, it can easily integrate either the PM or the
 77 PR for straightforwardly modulating or resetting the CPG' phase. Detailed descriptions are provided in the
 78 following.

79 2.1.1 Decoupled neural SO (2)-based CPGs

80 Four decoupled neural SO (2)-based CPGs were used to produce multiple periodic signals for driving
 81 the quadruped robot (see Figure 1). Each neural SO (2)-based CPG consists of two connected neurons,
 82 where their neural activities are later adjusted by the PM or PR. It outputs two periodic signals that are
 83 transferred by a motor preprocessing unit to drive the hip 2 and knee joints of a leg. As a result, the leg's
 84 foot can trace a proper ellipse-like trajectory with swing forward and stance backward. The foot movement
 85 status detected by the GRF is transferred to the PM or PR through a sensory preprocessing unit. Based on
 86 the GRF feedback, the PM or PR generates modulation signals to its corresponding CPG. In the single
 87 closed-loop CPG-based control, the outputs of the CPG coordinate the two joint movements of the leg (i.e.,
 88 intralimb coordination), while the interlimb coordination among legs is realized only by the interactions
 89 between the robot body dynamics and the environment (i.e., physical communications) through the PM
 90 (Owaki et al., 2013) or PR (Aoi et al., 2012) with GRF feedback of each leg. This is because the four CPGs
 91 are decoupled and have no direct neural communication between them. The four CPGs can be described
 92 using a matrix in discrete time equations as follows:

$$\mathbf{a}(n+1) = \mathbf{w} \cdot \mathbf{o}(n) + \mathbf{b} + \mathbf{f}(n) \quad (1)$$

$$\mathbf{o} = \tanh(\mathbf{a}), \quad (2)$$

93 where $\mathbf{a} = (a_{ik})$, $\mathbf{o} = (o_{ik})$, and $\mathbf{b} = (b_{ik}) \in \mathbb{R}^{2 \times 4}$ represent the activations, outputs and biases of the
 94 CPG neurons, respectively. Each column of the three matrix variables (i.e., \mathbf{a} , \mathbf{o} , and \mathbf{b}) represents the
 95 values of a CPG. Moreover, n indicates the time of the discrete-time equations, where the update frequency
 96 is 60 Hz in the following investigations. $\mathbf{w} \in \mathbb{R}^{2 \times 2}$ is the synaptic weights of a CPG (see Equation (4)).
 97 $\mathbf{f} = (f_{ik}) \in \mathbb{R}^{2 \times 4}$ represents the modulation term of the PM or PR (see Equations (6), (7), and (8)). f_{ik} is
 98 the PM or PR term projecting to the i th neuron of the k th CPG. The projection can adjust the CPG neuron
 99 activities online, thereby resulting in the CPG phase adaptation.

100 The CPG outputs (\mathbf{o}) are used to drive the joint movements through a linear transformation of the motor
 101 preprocessing unit (see Figure 1). It is given by the following equation:

$$\boldsymbol{\theta} = \boldsymbol{\alpha} \mathbf{o} + \boldsymbol{\beta}, \quad (3)$$

102 where $\boldsymbol{\theta}$ and $\boldsymbol{\beta} \in \mathbb{R}^{2 \times 4}$ represent the desired joint angles and their biases, respectively.

103 Based on previous work (Manoonpong et al., 2013), each SO (2)-based CPG can generate periodic
104 coordinated signals for intralimb and interlimb coordination by setting its weights and biases as follows:

$$\mathbf{w} = \begin{pmatrix} 1.4 & 2.6 \\ -2.6 & 1.4 \end{pmatrix}, \quad (4)$$

$$\mathbf{b} = \begin{pmatrix} 0.01 & 0.01 & 0.01 & 0.01 \\ 0.01 & 0.01 & 0.01 & 0.01 \end{pmatrix}. \quad (5)$$

105 The CPGs' parameter setup is used for the following investigations.

106 2.1.2 Phase modulation (PM) mechanism

107 The fundamental principle of the PM is to modulate the CPG phase continuously by relying on the
108 continuous GRF signal. Based on the model of the neural SO (2)-based CPG with sensory feedback
109 introduced by (Barikhan et al., 2014), a modified version of the sensory feedback is proposed. It is
110 formulated as the PM modulation term in the following equations:

$$f_{ik}(n) = \begin{cases} -\gamma \frac{F_k(n)}{mg} \cos(o_{ik}(n)), & i = 1, \\ -\gamma \frac{F_k(n)}{mg} \sin(o_{ik}(n)), & i = 2, \end{cases} \quad (6)$$

111 where o_{ik} is the output of the i th neuron in the k th CPG, γ is a positive constant that represents the sensory
112 feedback gain, and F_k is the GRF value whose range depends on the specific robot weight. Here, mg
113 represents the weight of the robot. It is 2.5 kg for the robot used in the investigations. The robot weight is
114 introduced to normalize the sensory feedback gain for generalization. In addition, γ is a dimensionless
115 parameter that is independent of the robot.

116 From Equation (6), one can find that the greater the $F_k(n)$ a leg perceives, the higher the inhibition (if
117 $f_{ik}(n) < 0$) or excitation (if $f_{ik}(n) > 0$) the corresponding leg's PM makes. More specifically, when
118 the robot is on the ground, its four legs support and promote the robot body together. Thus, there is an
119 approximately equal distribution among the GRFs of the four legs during locomotion. This means that,
120 when the GRF of a stance leg decreases, the GRFs of other stance legs must increase. Therefore, the four
121 CPGs have different modulation strengths. This results in phase differences among the four CPGs. Once
122 the CPG phase differences converge to a proper status, adaptive interlimb coordination (i.e., self-organized
123 locomotion) emerges (Owaki et al., 2013; Sun et al., 2018).

124 2.1.3 Phase resetting (PR) mechanism

125 The fundamental principle of the PR is to reset the CPG phase intermittently by relying on the discrete
126 GRF signal. For neural SO (2)-based CPG, the PR functionality is realized by resetting the CPG neuron
127 activities to specific values when the GRF value increases over a threshold. Thus, the PR modulation term
128 can be described as follows:

$$f_{ik}(n) = \begin{cases} (1 - (w_{11}o_{1k}(n) + w_{12}o_{2k}(n) + b_{1k}))\kappa, & i = 1, \\ -(w_{21}o_{1k}(n) + w_{22}o_{2k}(n) + b_{2k})\kappa, & i = 2, \end{cases} \quad (7)$$

$$\kappa = \begin{cases} 1.0, & F_k(n) > F_t \frac{mg}{4}, \quad F_k(n-1) \leq F_t \frac{mg}{4} \\ 0.0, & \text{otherwise} \end{cases}, \quad (8)$$

131

132 where o_{ik} is the activity/output of the i th neuron in the k th CPG, mg is the weight of the robot, and F_t is a
 133 positive value representing GRF threshold factor that influences the timing of the PR. Here, $\frac{mg}{4}$ is regarded
 134 as a reference GRF value given that the four legs share the support of the robot weight. Once the GRF
 135 ($F_k(n)$) of a leg becomes more than $\frac{mg}{4}$, the leg is indicated to be in the stance phase, thereby triggering
 136 the PR. Thus, to realize proper phase resetting, F_t value can be easily set in a small range approximately
 137 1.0. Moreover, F_t is a dimensionless parameter that is independent of the robot.

138 More specifically, the condition in Equation (8) indicates that once the GRF value of a leg increases over
 139 $F_t \frac{mg}{4}$, then κ of the leg (e.g., the k th leg) is equal to 1.0. As a result,

$$f_{ik}(n) = \begin{cases} 1 - (w_{11}o_{1k}(n) + w_{12}o_{2k}(n) + 0.01), & i = 1, \\ -(w_{21}o_{1k}(n) + w_{22}o_{2k}(n) + 0.01), & i = 2, \end{cases} \quad (9)$$

140 Replacing them into Equations (1) and (2), the k th neural SO(2)-based CPG outputs at the next step are
 141 approximately reset to:

$$\begin{aligned} & o_{ik}(n+1) = \tanh(a_{ik}(n+1)) \\ = & \begin{cases} \tanh(w_{11}o_{1k}(n) + w_{12}o_{2k}(n) + 0.01 + 1 - (w_{11}o_{1k}(n) + w_{12}o_{2k}(n) + 0.01)), & i = 1, \\ \tanh(w_{21}o_{1k}(n) + w_{22}o_{2k}(n) + 0.01 - (w_{21}o_{1k}(n) + w_{22}o_{2k}(n) + 0.01)), & i = 2, \end{cases} \\ & = \begin{cases} \tanh(1), & i = 1, \\ \tanh(0), & i = 2, \end{cases} \\ & \approx \begin{cases} 0.76, & i = 1, \\ 0, & i = 2, \end{cases} \end{aligned} \quad (10)$$

142

143 The CPG outputs are reset to the approximation from its limit cycle when a phase-resetting event occurs,
 144 followed by the CPG outputs returning to its limit cycle (see Figure 3 (A)). Owing to the differences among
 145 the four GRFs, the phases of the CPGs are reset at different moments, thereby having phase differences.
 146 For example, when the robot wriggles with four legs supporting it on the ground, the GRFs of the four legs
 147 are close to $F_t \frac{mg}{4}$. In this case, the robot torso twisting back and forth leads to the GRFs with different
 148 change tendencies (e.g., front leg GRFs increase while hind leg GRFs decrease), which results in the GRFs
 149 of the legs meeting the PR condition at different moments. When the CPG phase differences converge to a
 150 proper status, adaptive interlimb coordination (i.e., self-organized locomotion) emerges (Aoi et al., 2010,
 151 2012). More detailed information on the locomotion generation process can be found in the following
 152 experiments and corresponding videos.

153 2.2 Experimental platform

154 The experimental platform for studying the PM and PR is a quadruped robot in the simulation. The
 155 simulated robot is based on a small-size quadruped robot with multiple sensory feedback (Lilibot) which
 156 was developed in our previous works (Sun et al., 2020). The simulation environment was built using
 157 CoppeliaSim² with physical engine Vortex³. The framework for connecting the robot with the adaptive
 158 neural controller (including the PM or PR) is based on the robot operation system (ROS)⁴ (see Figure 2).

² <https://www.coppeliarobotics.com/>

³ <https://www.cm-labs.com/vortex-studio/>

⁴ <https://www.ros.org/>

159 The robot and controller are regarded as two ROS nodes and communicate with each other through two
 160 ROS topics. A motor topic is used to transfer commands from the controller node to the robot node, while
 161 a sensory topic is used to acquire GRF signals from the robot node and then send them to the controller
 162 node. The update frequency of the two ROS nodes is 60 Hz, the CoppeliaSim calculation time step is 50
 163 ms (20 Hz) during which main script of the simulated models is executed once. The simulation runs on a
 164 laptop (Thinkpad E470C) setup with an Intel Core i5-7200U and 8GB DDR4. The detailed information and
 165 source of the robotic platform can be found at <https://gitlab.com/neutron-nuaa/lilibot>.
 166 The launch sequence of the modules in the simulation is the CoppeliaSim initially and the two ROS nodes
 167 after 60 steps (3 s in CoppeliaSim).

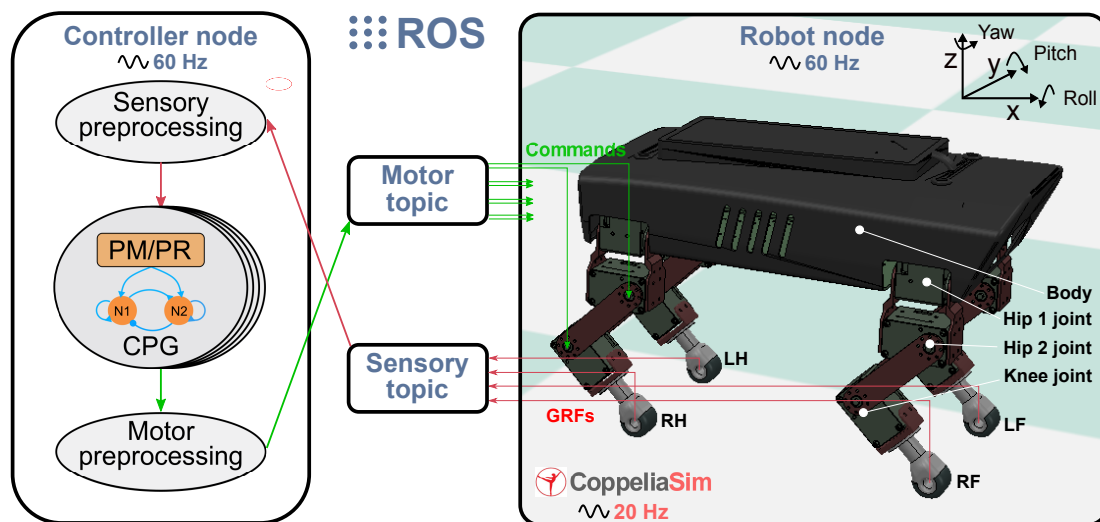


Figure 2. Experimental platform with the quadruped robot in CoppeliaSim (20Hz) communication with the adaptive neural controller. The controller and the robot are regarded as two ROS nodes (60 Hz) and communicate with each other through two ROS topics. A motor topic transfers commands from the motor preprocessing unit of the controller node to the robot joints while a sensory topic acquires GRF signals from the robot and then send them to the sensory preprocessing unit of the controller node.

168 2.3 Measurement of CPG phase convergence and self-organized locomotion

169 In this study, we focused on the autonomous phase regulation of decoupled CPGs modulated by the
 170 PM and PR, resulting in quadruped self-organized locomotion. Here, we consider a neural SO(2)-based
 171 CPG with specific dynamical properties in which the CPG with a certain frequency exhibits a limit cycle
 172 similar to a unit circle in phase space, as shown in Figure 3 (A). In other words, the PM and PR are used to
 173 modulate the CPG phase rather than adapting to other properties (for example, amplitudes, offsets, and
 174 frequency). As a result, under the CPG parameter setup in Equations (4) and (5), the phase relationship of
 175 the decoupled CPGs converges to a certain state where the quadruped robot can form a specific gait (i.e.,
 176 trot-like gait).

177 To clearly analyze and assess the characteristics of the PM and PR for the CPG phase regulation, several
 178 variables and metrics (see Table 1) were introduced to measure their CPG phase convergence process and
 179 resulting self-organized locomotion (see Figure 3). The metrics were used to assess the PM and PR in the
 180 experiments. Because the variables are the basis of the metric definitions, the variables are here introduced
 181 in the following subsection first. They include the phase difference and its mean and standard deviation.

Table 1. List of the variables and defined metrics.

Variables	Symbols	Metrics	Symbols
Phase difference	$\phi_{kl}(n)$	Phase convergence time	T
Mean of phase difference	$\phi_{kl}^{mean}(n)$	phase deviation	ϕ^s
Standard deviation of phase difference	$\phi_{kl}^{std}(n)$	Cost of transport	COT
Sum of standard deviation of phase differences	$\phi^{std}(n)$		

182 2.3.1 Variables

183 A phase difference between two CPGs can identify the phase relationship of the two CPGs as well as the
 184 movement relationship between the two limbs/legs controlled by the two CPGs. The outputs of a CPG
 185 (e.g., o_{k1} and o_{k2}) at a moment can be illustrated as a point (P^k) in a phase diagram (see Figure 3 (A)). The
 186 two axes of the phase diagram represent the CPG outputs $o_{1,2}$. When the CPGs produce periodic signals
 187 (see Figure 3 (B)), their outputs follow their limit cycle to move. The limit cycle of a neural SO (2)-based
 188 CPG is similar to a circle whose origin is at the center of the coordinate. In the adaptive neural controller,
 189 the four neural SO (2)-based CPGs are identical with the same parameter values, so their limit cycles are
 190 the same in the phase diagram. Therefore, a phase difference (e.g., ϕ_{kl}) between two CPGs (i.e., the k th
 191 and l th CPGs) can be represented by the angle between the two points (i.e., P^k and P^l). Its mathematical
 192 description is as follows:

$$\phi_{kl} = \arccos\left(\frac{\mathbf{P}_k \cdot \mathbf{P}_l}{\|\mathbf{P}_k\| \|\mathbf{P}_l\|}\right), \quad (11)$$

193 where \mathbf{P}_k and \mathbf{P}_l represent the vectors of the k th and l th CPGs in the phase diagram, respectively
 194 (Figure 3 (A)). $\phi_{kl} \in [0, \pi]$ represents the magnitude of their (relative) phase difference. Based on this
 195 definition (ϕ_{kl}), when the adaptive neural controller is implemented on the quadruped robot to generate
 196 self-organized locomotion (Figure 3 (D)), one can find the phase differences (i.e., ϕ_{12} and ϕ_{13}) change
 197 from in phase to stable phase relationships (Figure 3 (B)). As a result, the phase differences among
 198 the CPGs can display their phase relationship online (see Figure 3 (C)). A video to show the phase
 199 difference convergences of the four decoupled CPGs modulated by the PM and PR can be seen in
 200 <http://www.manoonpong.com/AICM/video1.mp4>.

201 The phase differences undulate during the phase convergence process. To monitor the undulation, the
 202 mean and standard deviation of the phase differences are introduced. Because $\phi_{kl} \in [0, \pi]$ changes in a
 203 linear manner, it can be regarded as linear data rather than circular data when calculating its statistical
 204 variables. Thus, the mean and standard deviation are described as follows:

$$\phi_{kl}^{mean}(n) = \begin{cases} \frac{1}{N} \sum_{i=n-N}^n \phi_{kl}(i), & n > N \\ \frac{1}{n} \sum_{i=0}^n \phi_{kl}(i), & n \leq N \end{cases}, \quad (12)$$

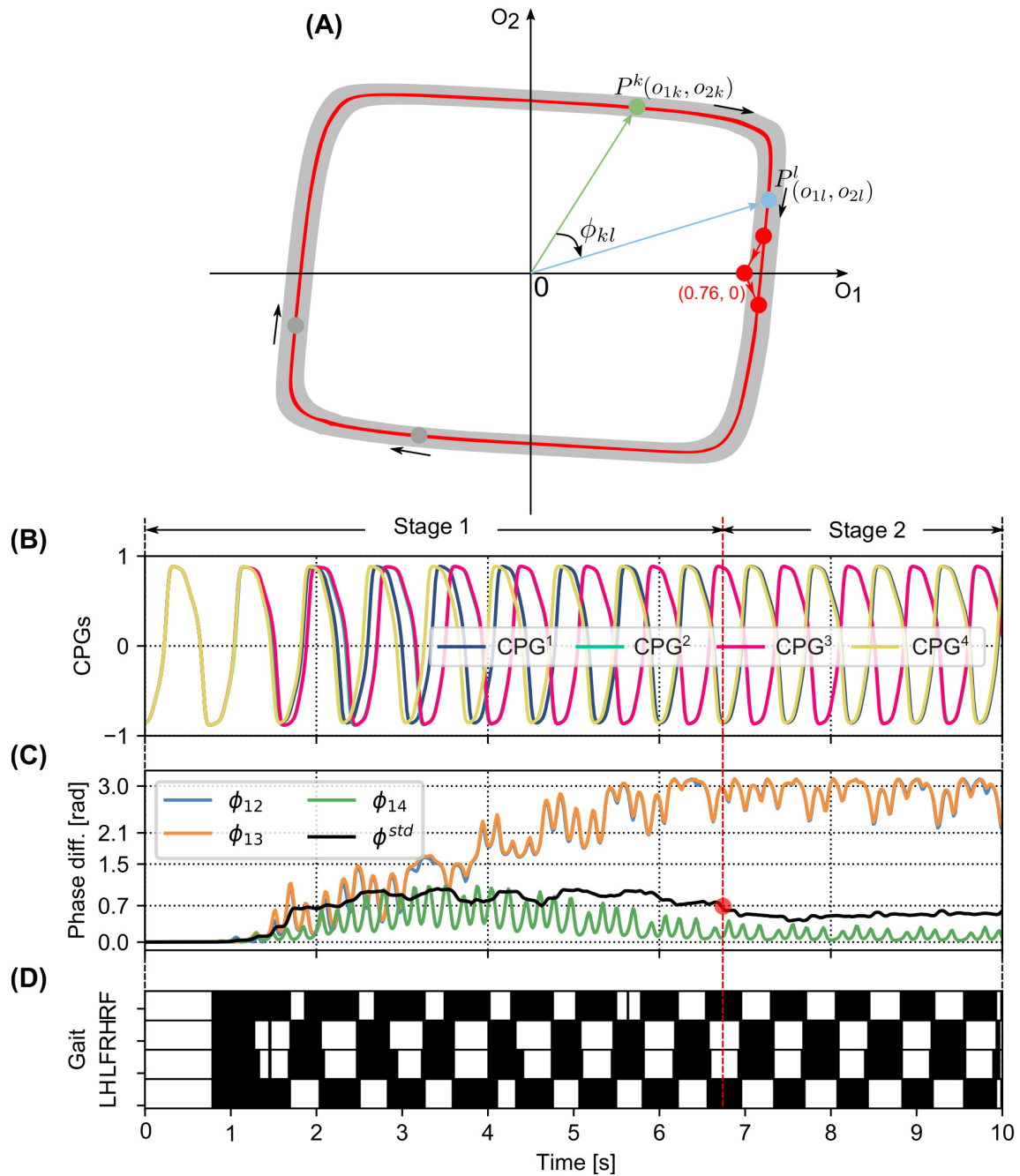


Figure 3. (A) The limit cycle of the $SO(2)$ -based CPGs that was used to investigate the autonomous phase regulation. The coordinates $(0.76, 0)$ represent the phase-reset point realized by the PR. A phase difference (e.g., ϕ_{kl}) between two CPGs (i.e., the k th and l th CPGs) is defined as the angle between the two points (i.e., P^k and P^l). (B) The first neuron outputs (o_{1k} with $k=1, 2, 3,$ and 4) of the four CPGs that are used to control the four legs, respectively (see Figure 1). (C) The CPG phase differences (i.e., ϕ_{12} , ϕ_{13} , ϕ_{14}) and their standard deviation (ϕ^{std}). ϕ^{std} can indirectly reflect the phase deviation. Empirically, once the value of ϕ^{std} reduces to less than 0.7 (see the red point), the CPG outputs and phase differences become more stable. The CPG phase convergence process can be divided into two stages (Stage 1 and Stage 2) determined by the point. (D) In the corresponding gait diagram, the black areas indicate stance phases while the white areas indicate swing phases. Note that, ϕ_{12} , ϕ_{13} , and ϕ_{14} are the phase differences of the CPG², CPG³ and CPG⁴ with respect to the CPG¹, respectively. RF, RH, LF, and LH are the right front, right hind, left front, and left hind legs, respectively.

$$\phi_{kl}^{std}(n) = \begin{cases} \frac{1}{N} \sqrt{\sum_{i=n-N}^n (\phi_{kl}(i) - \phi_{kl}^{mean}(n))^2}, & n > N \\ \frac{1}{n} \sqrt{\sum_{i=1}^n (\phi_{kl}(i) - \phi_{kl}^{mean}(n))^2}, & n \leq N \end{cases}, \quad (13)$$

$$\phi^{std}(n) = \sum_{l=2}^4 \phi_{1l}^{std}(n), \quad (14)$$

205 where $\phi_{kl}^{mean}(n)$ and $\phi_{kl}^{std}(n)$ are the mean and standard deviation of the phase difference ϕ_{kl} at current step
 206 n , respectively. N is the number of steps in a period from the current to a previous step. It is empirically
 207 set to 50 in the following experiments. Here, $\phi^{std}(n)$ is the sum of $\phi_{12}^{std}(n)$, $\phi_{13}^{std}(n)$, and $\phi_{14}^{std}(n)$ at the
 208 n th step. This can reflect the instantaneous/current deviation of the phase differences in overall. The less
 209 $\phi^{std}(n)$, the higher the phase deviation at the n th step.

210 To identify whether the CPG phase relationships are so stable that self-organized locomotion is recognized
 211 to be formed, according to the instantaneous indication of the phase deviation ($\phi^{std}(n)$), a constant ϕ_t^{std} is
 212 introduced as a threshold for distinguishing the phase convergence process. It is empirically set to 0.7 in
 213 the following experiments.

214 2.3.2 Metrics

215 Based on the proposed variables (see Table 1), the first metric is phase convergence time, which indicates
 216 how long the CPG phase relationship takes to converge and the robot takes to generate self-organized
 217 locomotion under the restrict conditions. **The state transition of the decoupled CPGs with the PM/PR from**
 218 **the initial fixpoint (0, 0, 0) to the desired fixpoint (π , π , 0) is accompanied by a process in which ϕ^{std} first**
 219 **increases and then decreases. Based on many experiments, we realize that if ϕ^{std} first reduces to less than a**
 220 **threshold ($\phi_t^{std}=0.75$) from a high value, the dynamical system will converge, and the quadruped robot can**
 221 **form a trot-like gait. Thus, the phase convergence time (T) is described as:**

$$T = \frac{\min(n_i)}{H}, \quad \phi^{std}(n_i - 1) \geq \phi_t^{std}, \quad \phi^{std}(n_i) < \phi_t^{std}, \quad (15)$$

222 where ϕ_t^{std} is the threshold. n_i is the step when ϕ^{std} is reduced to less than ϕ_t^{std} in a trial, whereas $\min(n_i)$
 223 is the minimal value of n_i and represents the step when ϕ^{std} first reduces to less than the threshold. H is
 224 the update frequency of the control node (i.e., 60 Hz).
 225

226 The second metric is *phase deviation*, which estimates the deviation of the phase differences. It can
 227 reflect the extent to which the converged CPG phase relationships are sustained during a self-organized
 228 locomotion period. It is defined using the reciprocal of the mean of $\phi^{std}(n)$ as follows:

$$\phi^s = \frac{1}{\text{mean}(\phi^{std}(n))}, \quad \text{mean}(\phi^{std}(n)) \neq 0, \quad (16)$$

229 where $mean(\phi^{std}(n))$ represents the mean of ϕ^{std} in the period (e.g., with M steps). The greater ϕ^s , the
 230 higher the phase deviation of the formed self-organized locomotion over the period.

231 The last metric is the *cost of transport (COT)*. It is used to measure the energy efficiency of the formed
 232 self-organized locomotion over a period. The COT is described as bellows:

$$\begin{cases} COT = \frac{E}{mgd}, \\ E = \sum_{j=1}^{12} \sum_{n=1}^M \frac{I_j(n)V_j(n)}{H}, \end{cases} \quad (17)$$

233 where E is the energy consumption when the robot with weight mg travels with a distance d . The energy is
 234 calculated using the robot joint motor current $I_j(n)$ and voltage $V_j(n)$. M indicates the number of steps
 235 over the period. H is the update frequency of the experimental system.

3 EXPERIMENTAL RESULTS

236 To systematically analyze and compare the characteristics of the PM and PR for self-organized locomotion,
 237 three robot experiments were conducted to measure the proposed metrics. First, the phase convergence time
 238 (see Equation (15)) of the PM and PR under different parameter values was investigated. Subsequently, the
 239 phase convergence time of the PM and PR under different robot situations (i.e., a normal situation as a
 240 baseline, noisy feedback, leg damage, and carrying a load) were compared. Finally, the phase deviation
 241 (see Equation (16)) and COT (see Equation (17)) under the robot situations were also studied. More than
 242 15 trials were conducted for each experiment under each mechanism (i.e., the PM or PR). Each trial was
 243 performed for more than 35 s.

244 **At the beginning of each trial, an identical initialization procedure was conducted to maintain all**
 245 **experimental trials with the same initial conditions when the PM/PR was activated (initial state). The**
 246 **initialization required 270 time steps of 13.5 s, from the start of the simulation ($n = 0$) to the moment**
 247 **of dropping the robot on the ground ($n = n_0$, where $n_0 = 270$ in the following experiments). This**
 248 **initialization duration was selected to provide sufficient time to fulfill three settings: 1) setting/initializing**
 249 **the GRFs ($F_k(n_0)$) to zero by holding the robot in the air; 2) setting the joints of the four legs to the initial**
 250 **positions ($\theta_{ik}(n_0)$) at the beginning of the simulation in all trials, so that the four legs had the same initial**
 251 **movement when the robot was dropped on the ground; 3) setting the CPG weights and biases to the initial**
 252 **values shown in Equations (4) and (5). The four neural SO(2)-based CPGs had the same parameter values**
 253 **and performed as the quasi-periodic attractors (see Figure 3 (A)). As a result, the four CPGs generated**
 254 **stable periodic signals ($o_{ik}(n_0)$) in phase to control leg movement in the initial state (see Figure 3 (B)).**

255 3.1 Phase convergence time under different parameter values

256 From Equations (6) and (8), it is known that the PM and PR parameters (i.e., sensory feedback gain γ
 257 and force threshold factor F_t) play a key role in the CPG phase convergence. Therefore, this experiment
 258 investigated the optimal parameter values for fast CPG phase convergence through massive trials. To do
 259 that, the proposed adaptive neural controller with the PM or PR was applied to the robot. After initialization,
 260 the robot was placed on the ground, and it started to interact with the environment to form self-organized
 261 locomotion. The experimental results are depicted in Figures 4 and 5.

262 For the PM, a sequence of the sensory feedback gains from 0.0 to 1.0 was tested. The range of the gain
 263 (i.e., 0.04, 0.12, 0.2, 0.28, 0.36, and 0.4) is shown in Figure 4. The other parameter values are not shown
 264 because they cannot enable the CPG phase differences to converge in all 15 trials. In the figure, the phase

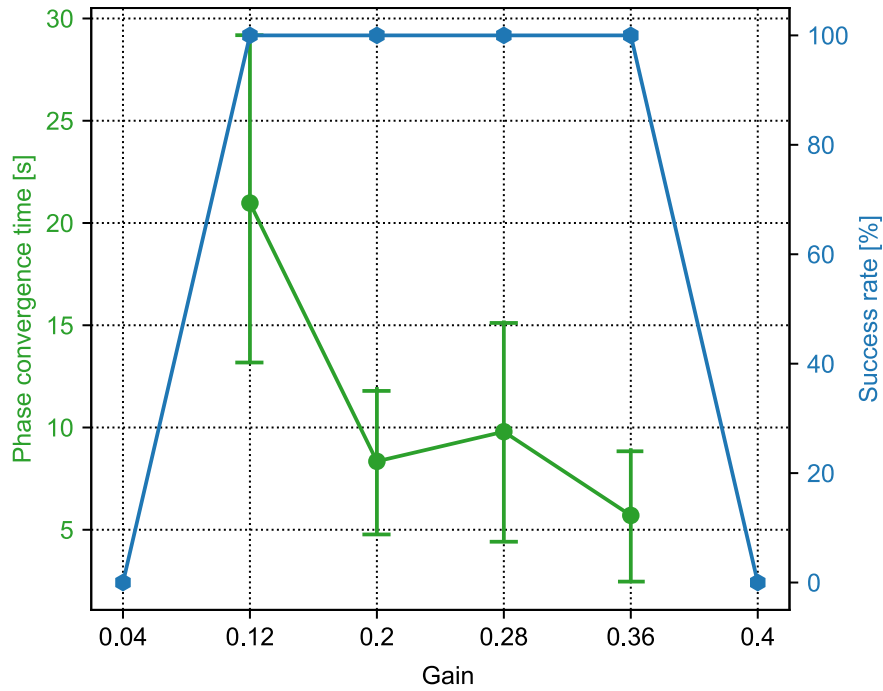


Figure 4. The phase convergence time and success rate of the PM trials with different sensory feedback gains (γ in Equation (6)). The green points and bars show the average and variance of the phase convergence time, respectively. The blue points represent the success rate. When the gain is 0.36, the success rate is 100% and has the fastest phase convergence.

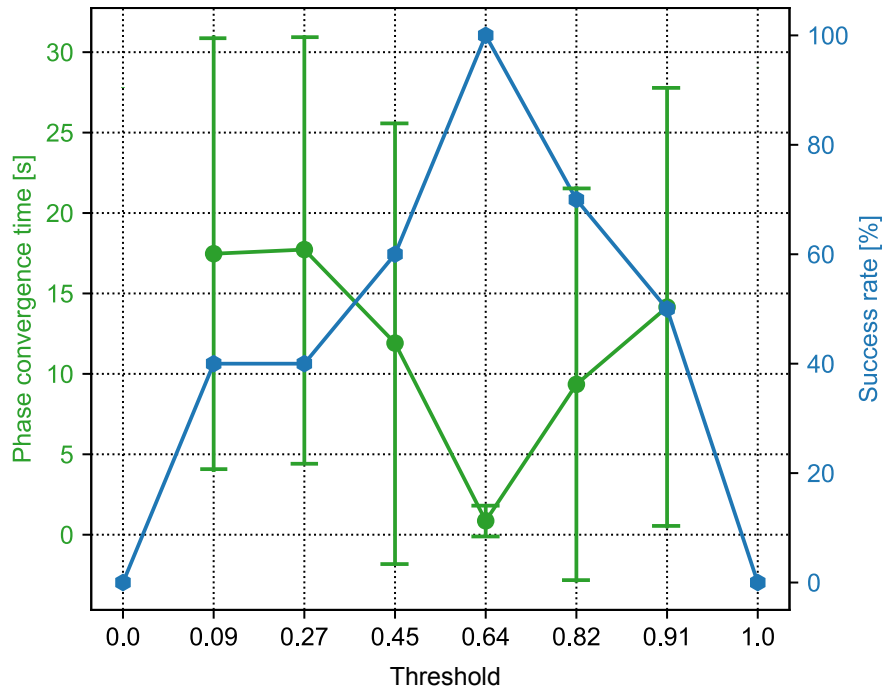


Figure 5. The phase convergence time and success rate of the PR trials with different force threshold factors (F_t in Equation (6)). The green points and bars show the average and variance of the phase convergence time, respectively. The blue points represent the success rate. When the threshold factor is 0.64, the success rate is 100% and has the fastest phase convergence.

265 convergence time and success rate within 15 trials were recorded. Obviously, when the gain is in the range
266 of [0.12, 0.36], the success rate is 100%. This means that the PM with these parameter values enables the
267 robot to generate self-organized gait robustly in all 15 trials. One can also find that the best value of the
268 gain is 0.36, by which the average phase convergence time is approximately 6 s. Consequently, the fastest
269 phase convergence speed of the PM can be realized by setting γ to 0.36. This value was used for the PM in
270 the following experiments.

271 For the PR, a sequence of the force threshold factor from 0.0 to 1.5 was tested. The range of the threshold
272 (i.e., 0.0, 0.09, 0.27, 0.45, 0.64, 0.82, 0.91, and 1.0) is shown in Figure 5. The other parameter values are
273 not shown because they cannot enable the CPG phase differences to converge in all 15 trials. In the figure,
274 the phase convergence time and success rate within 15 trials were recorded. Obviously, when the threshold
275 factor is in the range of [0.09, 0.91], the success rate is greater than or equal to 40%. Especially, when the
276 threshold factor is 0.64, the success rate is 100%. This means that the PR with the parameter value enables
277 the robot to generate self-organized gait robustly in all 15 trials. In addition, the corresponding average
278 phase convergence time is just approximately a second with a small derivation. Consequently, 0.64 is the
279 optimal parameter value of the PR for the fastest phase convergence speed. This value was also used for
280 the PR in the following experiments.

281 A success rate of 0% and 100% implies that the robot could not and could perform self-organized
282 locomotion in all 15 trials. The basis for determining whether the robot forms self-organized locomotion
283 (walking pattern) is that the phase differences (ϕ_{12} , ϕ_{13} , ϕ_{14}) among the four CPGs converge to particular
284 states around the desired fixpoint ($\pi, \pi, 0$) or the sum of their standard deviation (ϕ_{std}) first reduces to less
285 than a threshold (i.e., 0.7). For example, if the robot can perform a trot-like gait, the phase differences
286 (ϕ_{12} , ϕ_{13} , ϕ_{14}) should converge to approximately ($\pi, \pi, 0$) (see Figures S1 and S2 in the supplementary
287 material).

288 3.2 Phase convergence time in different situations

289 The sensory feedback, GRF information, plays an essential role in the function of the PM and PR. To
290 observe the adaptation of the PM and PR with respect to the GRFs, the PM and PR were examined in
291 different robot situations, in which the robot might perceive different GRFs. The situations are illustrated
292 in Figure 6. Their description can be seen in Table 2.

293 The abnormal situations (S2, S3, and S4) were used to compare the functional properties of the PM and
294 PR. The parameter settings of the abnormal situations were determined empirically to distinguish them
295 from the normal situation (S1). In the S2 situation, Gaussian-distributed noise was empirically determined
296 based on a trade-off between significant noise effects and the undisturbed phase regulation function of the
297 PM and PR. Consequently, we used Gaussian distributed noise with a standard deviation of 20% of the
298 GRFs. In the S4 situation, the weight of the payload was selected based on a trade-off between obviously
299 distinct GRFs of the legs and the robot load capability.

300 The experiments were also performed by implementing the adaptive neural controller with the PM or
301 PR on the quadruped robot but in the four situations. A video to show the robot generating self-organized
302 locomotion under the PM and PR in the four situations are shown in <http://www.manoonpong.com/AICM/video2.mp4>. The experimental results can be seen in Figure 7.

304 For the PM, the average phase convergence time is less than 3 s in all situations. The best performance is
305 in the S3 situation with the lowest average and variance of the phase convergence time, while the worst
306 is in the S2 situation with the largest variance. Moreover, some trials in the S2 situation require more

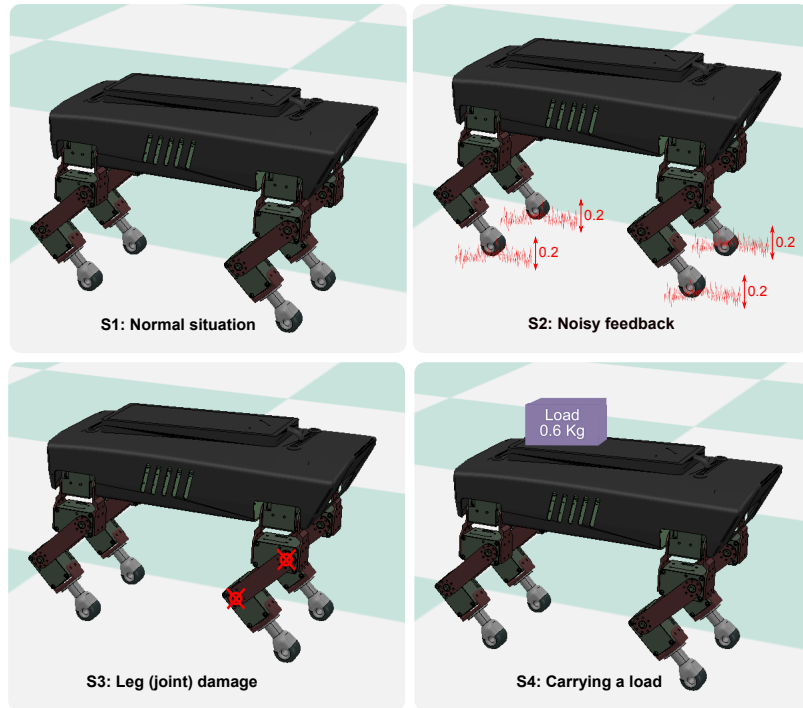


Figure 6. Four different situations that the robot experienced in the experiments. S1 was a normal situation. In S2, the GRFs of the four legs were added with Gaussian noise. In S3, the hip joint and knee joint of the right front leg were fixed to imitate leg damage. In S4, the robot carried a load of 0.6 kg.

Table 2. The description of the four different situations that the robot experienced in the experiments.

Situations	Description
S1 (normal situation)	This was a normal situation. It served as a baseline for comparison with other unexpected situations.
S2 (noisy feedback)	The GRFs of four legs were added with Gaussian noise with an amplitude of 20% of the maximum value of the GRFs.
S3 (leg damage)	The hip and knee joints of the right front leg were fixed, so the right front leg was unable to move during the experiments.
S4 (carrying a load)	The experiment robot (Lilibot) carried a 0.6 kg load, and the load was near its hind legs.

307 than 6 s to realize phase convergence. Overall, the unexpected situations (i.e., S2, S3, and S4) have faster
 308 phase convergence than that of the normal situation (S1). This is because the unexpected situations induced
 309 significant differentiation among the GRFs which can speed up the phase difference convergence.

310 For the PR, the phase convergence time of every situation in some trails is less than a second. Moreover,
 311 the average phase convergence time is less than 2 s, except for in the S2 situation, which exhibits the worst
 312 performance with the largest average and variance of the phase convergence time. Some trails cost more
 313 than 7 s to realize phase convergence in the S2 situation. This is because the added sensory noise made the
 314 GRFs randomly cross the force threshold so that the regular phase resetting process was destroyed. In the
 315 worst case, the CPG phase would never be reset.

316 To compare the results, the PR shows faster phase convergence than the PM on average, except for the
 317 trials in the S2 situation. This is because the PR rapidly reset the CPG phases once the GRFs increased

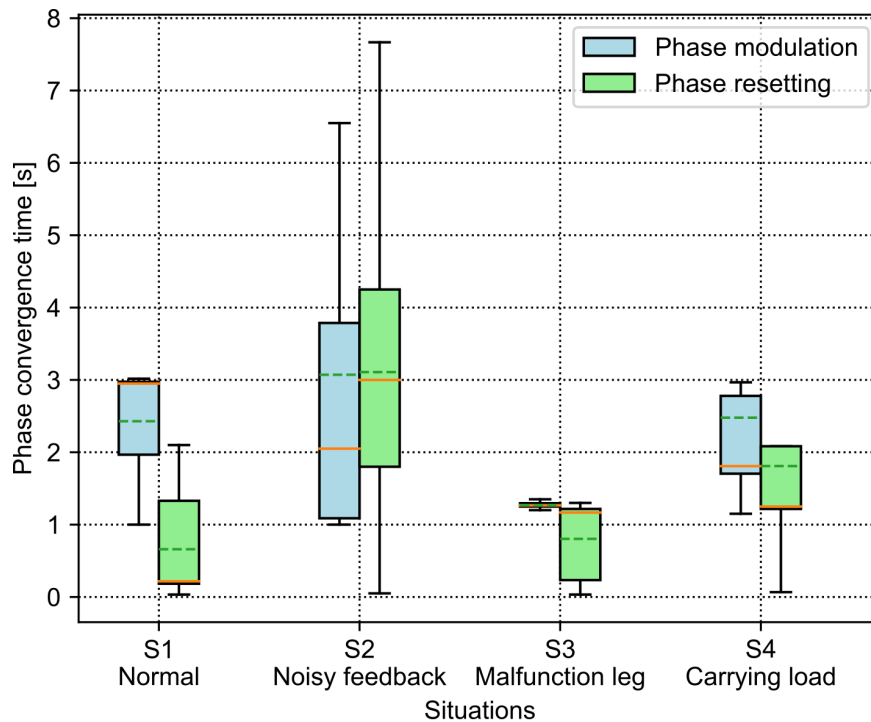


Figure 7. Phase convergence time of the PM and PR in four different situations. The solid and dashed lines in the boxes indicate the median and mean values of the phase convergence time, respectively.

318 over the threshold (i.e., 0.64) while the PM utilized the continuous GRFs with the gain (i.e., 0.36) to adjust
 319 the CPG phases smoothly. Consequently, the continuous phase modulation of the PM can cause slower
 320 but stable phase convergence. The rapid but intermittent phase resetting of the PR can cause faster phase
 321 convergence but with random success.

322 3.3 Phase deviation and COT in different situations

323 After the CPG phase differences (ϕ_{kl}) converge, the robot exhibits self-organized locomotion. It is also
 324 important to study how the phase differences and the formed locomotion are maintained. Therefore, this
 325 experiment exploited the deviation of the converged phase differences and used energy efficiency to assess
 326 the self-organized locomotion in the various situations.

327 The results of the phase deviation are shown in Figure 8. For the PM, the S1 situation has the greatest
 328 average phase deviation among the four situations. Specifically, the average phase deviation in the S1 and
 329 S2 situations is greater than 1.5, while it is less than 1.5 in the other two situations. For the PR, the S2
 330 situation has a large drop in the average phase deviation compared with the other situations. Specifically,
 331 the average phase deviation in the S1 and S2 situations is less than 1.75, while it is greater than 1.75 in the
 332 other two situations. Comparatively, the average phase deviation of the PM is higher than that of the PR in
 333 the S1 and S2 situations, but lower than that of the PR in the S3 and S4 situations.

334 The results of the energy efficiency (measured by COT) are shown in Figure 9. For the PM, the lowest
 335 and the highest average COT are in the S1 and S3 situations, respectively. Specifically, the average COT in
 336 the S1 and S2 situations is less than 0.9, while it is greater than 0.9 in the S3 and S4 situations. For the
 337 PR, the S2 situation has the highest COT in the four situations. Comparatively, the average COT of the
 338 PM is less than that of the PR in the S1 and S2 situations, but higher than that of the PR in the S3 and S4
 339 situations.

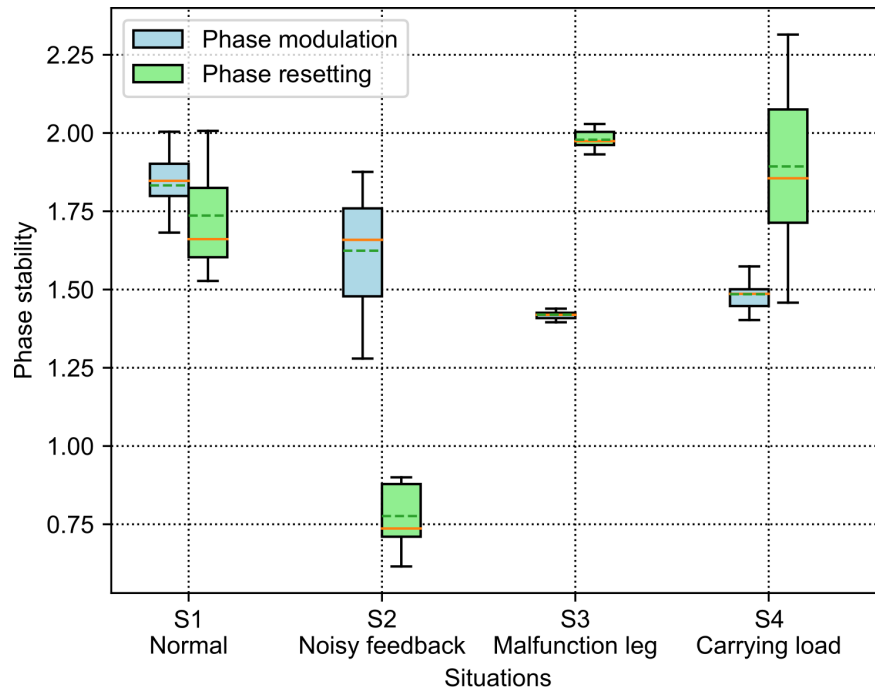


Figure 8. Phase deviation of the self-organized robot locomotion under the PM and PR in the four situations. The solid and dashed lines in the boxes indicate the median and mean values of the phase deviation, respectively.

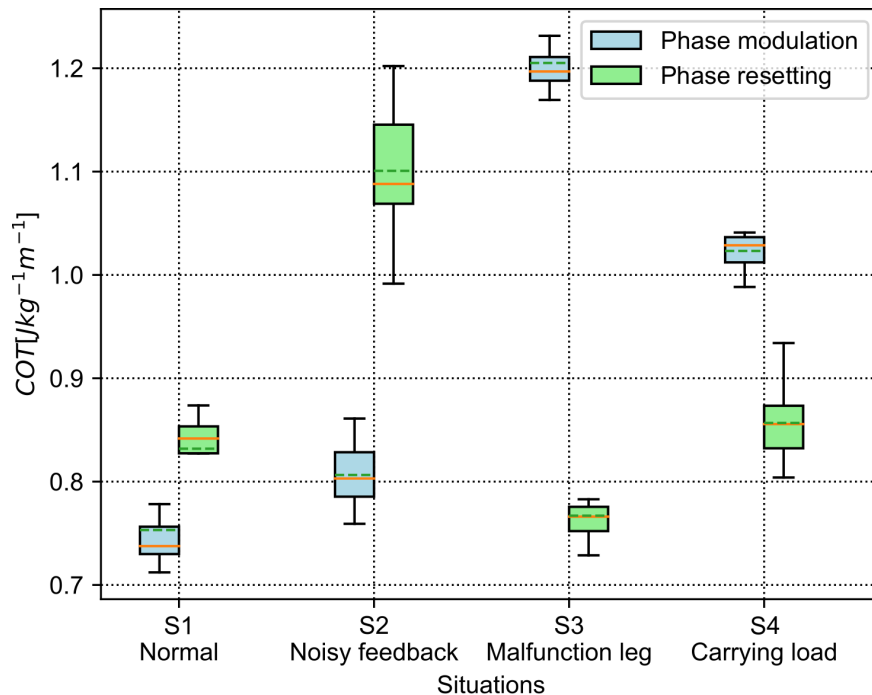


Figure 9. COT of the self-organized robot locomotion under the PM and PR in the four situations. The solid and dashed lines in the boxes indicate the median and mean values of the COT, respectively.

340 According to the results shown in Figures 8 and 9, the statistical analysis reveals that the PM has higher
 341 phase deviation and energy efficiency (lower COT value) than those of the PR in the S1 and S2 situations,
 342 while this result is reversed in the S3 and S4 situations.

343 Both the PM and PR have different performances (i.e., phase deviation and COT) in these situations. This
 344 results from the situations causing the robot to perceive different GRF distributions. The statistical GRFs
 345 under the PM and PR in the experiments are shown in Figures 10 and 11, respectively.

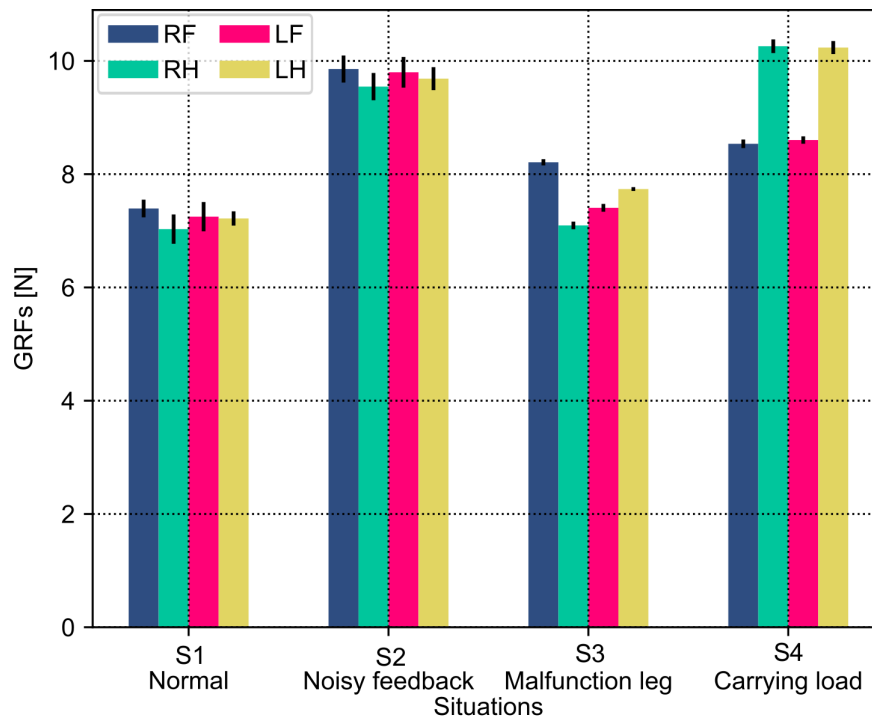


Figure 10. GRF distribution of the self-organized robot locomotion under the PM in four situations. Note that RF, RH, LF, and LH indicate the right front, right hind, left front and left hind legs, respectively.

346 In Figure 10, under the PM, the four legs (i.e., the RF, RH, LF, and LH legs) show more similar GRFs
 347 values in the S1 and S2 situations than in S3 and S4 situations. This phenomenon can also be seen in Figure
 348 11 under the PR. The GRF distributions of the four legs in the S1 and S2 situations are symmetric, while, in
 349 the S3 and S4 situations, the GRFs show relative asymmetry. Taken together, the PM shows higher phase
 350 deviation and energy efficiency when facing a symmetric GRF distribution, while the PR shows higher
 351 performance when facing an asymmetric GRF distribution.

4 DISCUSSION AND CONCLUSION

352 The aim of this study was to comparatively analyze the characteristics of the two classical adaptive
 353 interlimb coordination mechanisms, the PM (see Equation (6)) and PR (see Equation (7)), for autonomous
 354 CPG phase regulation and resulting self-organized locomotion and adaptation. The essential functions
 355 of the PM and PR represent two different ways to regulate the phase relationships among decoupled
 356 CPGs. Typically, the PM uses continuous GRFs to modulate CPG phases gradually while the PR uses
 357 discrete GRFs to reset the CPG phases intermittently. In this study, the two mechanisms were separately
 358 applied to the adaptive neural controller with four decoupled SO (2)-based CPGs (see Figure 1). They
 359 were implemented on the quadruped robot to experimentally assess the PM's and PR's parameters and
 360 adaptability to unexpected robot situations (see Figure 6). The experimental results indicate that 1) the PM
 361 and PR parameter values significantly influence the success rate and speed of the CPG phase convergences;
 362 2) overall, the PM exhibits slower but more stable phase convergence while the PR exhibits faster but less

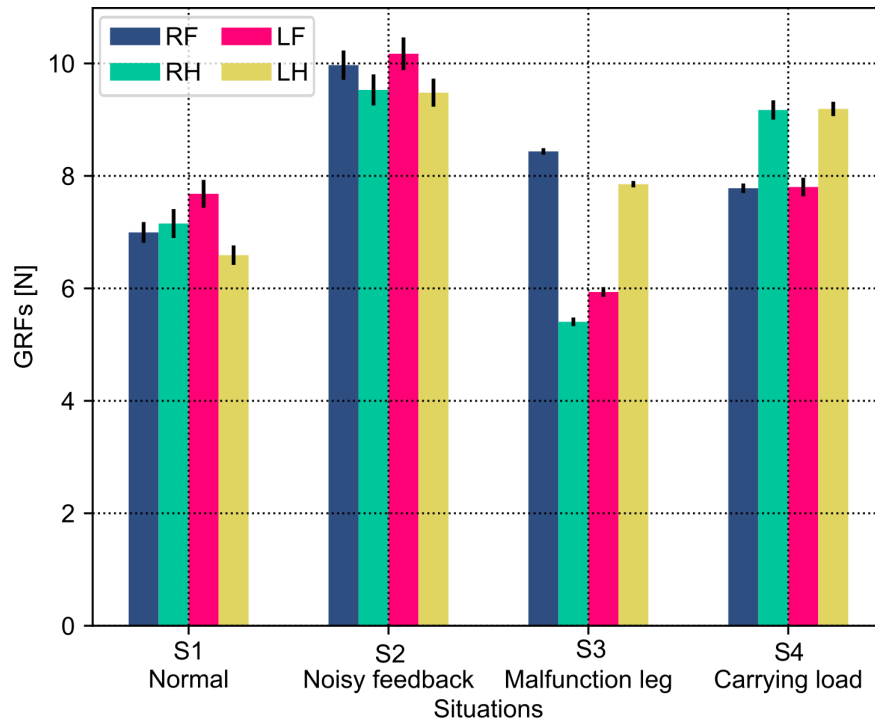


Figure 11. GRF distribution of the self-organized robot locomotion under the PR in the four situations. Note that RF, RH, LF, and LH indicate the right front, right hind, left front and left hind legs, respectively.

363 stable phase convergence (see Figures 4 and 5); 3) the CPG phase convergence time varies in different
 364 situations (see Figure 7); and 4) the PM and PR perform better when the robot is subjected to symmetrical
 365 and asymmetrical GRF distributions, respectively (see Figures 8, 9, 10, and 11).

366 The decoupled CPGs with the PM/PR form a complex dynamical system that comprises three sublevels.
 367 Its difference equations can be seen in Equations (1), (6), and (7). 1) The top sublevel dynamical system
 368 comprises four identical and decoupled CPGs with the PM or PR, the state variables of which are the
 369 CPG phase differences (i.e., ϕ_{12} , ϕ_{13} , and ϕ_{14}). 2) The middle sublevel dynamical system is a CPG with
 370 the PM or PR. The PM or PR term can be regarded as external adjustments on the CPG (basis sublevel
 371 dynamical system) when the robot interacts with the ground. 3) The basis sublevel dynamical system is
 372 a neural SO(2)-based CPG. Its state variables are the CPG outputs (o_{ik} , $i=1, 2$). Here, it is an oscillatory
 373 system under the proper parameter configuration (see Equations (4) and (5)). Its dynamics is a limit cycle
 374 in the phase space (see Figure 3 (A)). The initial conditions of a multiple-coupling CPG system strongly
 375 influence the convergence results (Dénes et al., 2019). In this work, the initial condition of the top sublevel
 376 dynamical system is the CPG coordination ($(o_{1k}(n_0), o_{2k}(n_0))$) at the CPG limit cycle when the robot
 377 lands on the ground ($n = n_0$). Thus, the ensemble of the initial conditions of the top dynamical system is
 378 the entire CPG limit cycle. In all experiments, we considered the initial condition of the time 270 steps
 379 ($n_0 = 270$) where $o_{1k}(n_0) \approx 0.836$ and $o_{2k}(n_0) \approx 0.067$.

380
 381 The convergence results (e.g., success rate) of the top sublevel dynamical system depend on the initial
 382 condition as well as the PM and PR parameter values (sensory feedback gain (γ) and GRF threshold
 383 (F_t)). When the PM and PR parameter values are outside their effective range (e.g., $\gamma \notin [0.12, 0.6]$ and
 384 $F_t \notin [0.09, 0.91]$, see Figures 4 and 5), the robot cannot achieve self-organized locomotion (success rate is
 385 0%) regardless of any initial condition. In this case, the top sublevel dynamical system always stays at an

386 initial fixpoint (0,0,0) (see Figure S1 and S2 in the supplementary material). This is because the PM and
387 PR with inappropriate parameter values cannot drive the system dynamics from the initial fixpoint to the
388 desired fixpoint ($\pi, \pi, 0$) where a gait can be formed. More specifically, for the PM, if $\gamma < 0.12$ (e.g., $\gamma = 0$,
389 Figure S3), the sensory feedback strength is extremely weak to modulate the CPG phase; if $\gamma > 0.6$ (e.g.,
390 $\gamma = 1$, Figure S5), the sensory feedback modulation is extremely strong, thereby significantly changing
391 the CPG properties (e.g., output amplitudes and offsets). For the PR, if $F_t < 0.09$ (e.g., $F_t = 0$, Figure
392 S6), the four CPG phases are reset at the same time so that their phase differences are zero; if $F_t > 0.91$
393 (e.g., $F_t = 1.5$, Figure S8), the four CPG phases never reset because the sensory feedback cannot meet the
394 phase-resetting condition.

395
396 The statistical results (success rate) of the self-organized locomotion are related to the initial condition
397 and parameter values. For the PM, if the parameter value (γ) is in the range of [0.12, 0.6], the PM-based
398 control enables the robot to generate self-organized locomotion with a 100% success rate. The experimental
399 real-time data of the case (e.g., $\gamma = 0.36$) are shown in Figure S4. The dynamical system converges to the
400 desired fixpoint ($\pi, \pi, 0$) in the phase space (see Figure S1). For the PR, if the parameter value (F_t) is in
401 the range of [0.09, 0.91], the PR-based control enables the robot to generate self-organized locomotion
402 (e.g., $F_t = 0.64$, Figure S7) with some uncertainties. The dynamical system can converge to the desired
403 fixpoint ($\pi, \pi, 0$) in the phase space (Figure S2). A slight difference in the initial condition may cause
404 distinct convergence results. For example, when F_t is 0.45, in one trial (Figure S9), the robot can perform
405 self-organized locomotion; in another trial using the same parameter value and the same initial procedure,
406 the robot cannot generate self-organized locomotion (see Figure S10). This is because, in the success case,
407 the GRFs of the four legs can cross the GRF threshold at slightly different times owing to slightly different
408 dynamics among the four legs at the touch moment, even when the four legs touch the ground at the same
409 time. This is because the GRFs of the four legs approached the GRF threshold with a slightly different
410 increase rate when the robot touched the ground (see Figure S9). According to this, the results based on the
411 PR are more sensitive to the initial condition than those based on the PM.

412 The cases with a 0% success rate in Figures 4 and 5 result from the inappropriate “physical
413 coupling strength” of the CPGs. In this work, the adaptive synchronizations/coordination among the
414 decoupled CPGs is realized via sensory feedback in the form of the PM or PR, which provides physical
415 communication/coupling effects on the CPGs. The PM and PR parameter values (γ of the PM and F_t of
416 the PR) determine the “physical coupling strength.” When the parameter values are extremely small or
417 large, the “physical coupling strength” also becomes extremely small or large such that synchronization
418 will not be achieved. As a result, the CPG phase relationships (ϕ_{12} , ϕ_{13} , and ϕ_{14}) of the decoupled CPGs
419 are not appropriate for forming a stable gait.

420 The PM and PR have been analyzed from various aspects in different ways in other works (Aoi et al.,
421 2012; Owaki et al., 2013, 2017; Ambe et al., 2018). For instance, in (Owaki et al., 2013), Owaki et al.
422 have summarized the spontaneous phase shift of the decoupled CPGs, which are regulated by local force
423 feedback in the form of the PM, as follows: (i) a phase delay is introduced in the CPG of each leg owing to
424 the physical effect of the local force feedback; (ii) this phase delay, which is introduced when the leg is in a
425 stance phase, allows time for other legs to enter the stance phase; (iii) as more legs begin to support the
426 body, the load on the support leg decreases; consequently, the feedback effect on the support leg decreases,
427 allowing it to enter the swing phase. The mechanism reveals how the phases of the CPG are appropriately
428 modified by local sensory feedback, resulting in the generation of the self-organized locomotion. In (Ambe
429 et al., 2018), Ambe et al. analyzed the phase evolution of (no direct interaction) ipsilateral oscillators,
430 which are regulated by local force feedback in the form of the phase resetting. In this case, the CPG phases

431 are shifted and converge to the final state when the legs touch the ground at proper moment. This is because
432 the force feedback can regulate the leg retraction timings by resetting the CPG phase.

433 However, in the above-mentioned studies the characteristics of the PM and PR models' parameters seem
434 to receive less attention and have not been reported in detail. In this work, the effects of the parameters
435 of the PM and PR on the CPG phase convergences were systematically investigated. As a result, their
436 optimal normalized parameter values were found (see Figures 4 and 5). This increases the practicality of
437 the two mechanisms for obtaining fast phase convergence in the normal situation (i.e., the S1 situation)
438 by reducing the manual parameter tuning. However, the phase convergence times vary in different robot
439 situations (see Figures 7). This suggests that adaptive parameter values of the PM and PR are necessary
440 in various situations. Recently, some studies have implemented learning techniques to obtain adaptive
441 sensory feedback gains of the PM mechanisms (Sun et al., 2018; Dujany et al., 2020; Miguel-Blanco and
442 Manoonpong, 2020).

443 Another important property of the PM and PR is their adaptability to changes in body properties. It has
444 been reported in many works (Owaki et al., 2013, 2017; Ambe et al., 2018), in which researchers have
445 reproduced certain impressive animal-like movements on legged robots, such as self-organized gaits and
446 autonomous gait transition in response to changes in body properties (e.g., leg amputations and weight
447 redistribution) and environments. These works viewed the adaptability in terms of adaptive walking patterns.
448 In this work, the phase deviation (Equation (16)) and energy efficiency (i.e., COT, see Equation (17)) were
449 exploited in four elaborated robot situations (see Figure 6).

450 The four situations varied the four legs' GRF amplitudes and exhibited two different GRF distributions:
451 symmetrical GRFs (in the S1 and S2 situations) and asymmetrical GRFs (in the S3 and S4 situations). The
452 experimental results show that the higher phase deviation of the CPGs corresponds to the higher energy
453 efficiency of the self-organized locomotion. This reflects a straightforward relationship of the control metric
454 to locomotion performance. The relationship maybe attributed to the higher phase deviation with fewer
455 unpredictable joint movement changes, thereby saving energy cost. Moreover, the PM and PR exhibited
456 good performance when they were subjected to symmetric and asymmetric GRF distributions, respectively.
457 This indicates that the two mechanisms should be selected in different situations in the self-organized robot
458 locomotion.

459 Taken together, the comparative study of the PM and PR in this work reveals not only the relationship
460 between their parameter values and the speed of the self-organized locomotion generation, but also the
461 preferred situations for high phase deviation and energy efficiency in locomotion. Based on this study, it
462 suggests that the PM and PR are effective in different situations. However, these conclusions are based on
463 the robot experiments with the specific neural SO(2)-based CPG setup and the simulated quadruped robot
464 platform. This limits the generality of the conclusions in general CPG and legged robots. In addition, the
465 definition of the phase convergence time depends on empirically tuned parameters (i.e., ϕ_t^{std} in Equation
466 (15) and N in Equation (12)), which were determined by observing the experiments implemented in our
467 specific robotic platform. As a result, the statistical results of the phase convergence time, phase deviation
468 (Figures 4 and 5, 7, and 8) could be affected by the experimental platform. Moreover, the metric ϕ_t^{std} is
469 not monotonic and could crossover the threshold more than once, for example, in the S2 situation where
470 the GRFs have additional noise (see Figure S16 in the supplementary material). Thus, to obtain the same
471 experimental conclusion on other experimental platforms, the empirical parameters should be adjusted
472 manually according to a specific experimental platform. Thus, in future work, we will further theoretically
473 investigate the two mechanisms based on a dynamical system perspective (Sándor et al., 2015; Martin et al.,
474 2016; Aguilar et al., 2016; Dénes et al., 2019) to further analyze the properties of the mechanisms (e.g.,

475 using Poincaré map (Owaki and Ishiguro, 2017)) and structural stability and to verify the experimental
476 results on other robotic systems, such as hexapod robots.

ACKNOWLEDGMENTS

477 The authors would like to thank Weijia Zong, Yan Li, and Potiwat Ngamkajornwiwat for their comments.
478 We also gratefully acknowledge the financial support of the NUAA research fund (Grant No. 1005-
479 YQRO7001, P.M., Project PI), NSFC-DFG Collaborative Research Program (Grant No. 51861135306,
480 P.M., project Co-PI), the National Natural Science Foundation of China (Grant No. 51435008 to Z.D), and
481 Chinese Government Scholarship (Grant No. CSC201906830012) [TS]).

REFERENCES

- 482 Aguilar, J., Zhang, T., Qian, F., Kingsbury, M., McInroe, B., Mazouchova, N., et al. (2016). A review on
483 locomotion robophysics: the study of movement at the intersection of robotics, soft matter and dynamical
484 systems. *Reports on Progress in Physics* 79, 110001
- 485 Ambe, Y., Aoi, S., Nachstedt, T., Manoonpong, P., Wörgötter, F., and Matsuno, F. (2018). Simple analytical
486 model reveals the functional role of embodied sensorimotor interaction in hexapod gaits. *PLOS ONE* 13,
487 1–28
- 488 Aoi, S., Egi, Y., Sugimoto, R., Yamashita, T., Fujiki, S., and Tsuchiya, K. (2012). Functional roles of
489 phase resetting in the gait transition of a biped robot from quadrupedal to bipedal locomotion. *IEEE*
490 *Transactions on Robotics* 28, 1244–1259
- 491 Aoi, S., Manoonpong, P., Ambe, Y., Matsuno, F., and Wörgötter, F. (2017). Adaptive control strategies for
492 interlimb coordination in legged robots: a review. *Frontiers in neurorobotics* 11, 39
- 493 Aoi, S. and Tsuchiya, K. (2007). Adaptive behavior in turning of an oscillator-driven biped robot.
494 *Autonomous Robots* 23, 37–57
- 495 Aoi, S., Yamashita, T., Ichikawa, A., and Tsuchiya, K. (2010). Hysteresis in gait transition induced by
496 changing waist joint stiffness of a quadruped robot driven by nonlinear oscillators with phase resetting.
497 In *2010 IEEE/RSJ International Conference on Intelligent Robots and Systems (IEEE)*, 1915–1920
- 498 Barikhan, S. S., Wörgötter, F., and Manoonpong, P. (2014). Multiple decoupled cpgs with local sensory
499 feedback for adaptive locomotion behaviors of bio-inspired walking robots. In *International Conference*
500 *on Simulation of Adaptive Behavior* (Springer), 65–75
- 501 Dénes, K., Sándor, B., and Néda, Z. (2019). Pattern selection in a ring of kuramoto oscillators.
502 *Communications in Nonlinear Science and Numerical Simulation* 78, 104868
- 503 Der, R. and Martius, G. (2012). *The playful machine: theoretical foundation and practical realization of*
504 *self-organizing robots*, vol. 15 (Springer Science & Business Media)
- 505 Dickinson, M. H., Farley, C. T., Full, R. J., Koehl, M., Kram, R., and Lehman, S. (2000). How animals
506 move: an integrative view. *science* 288, 100–106
- 507 Dujany, M., Hauser, S., Mutlu, M., van der Sar, M., Arreguit, J., Kano, T., et al. (2020). Emergent
508 adaptive gait generation through hebbian sensor-motor maps by morphological probing. In *International*
509 *conference of intelligent robots and systems (IROS)* (IEEE), 7866–7833
- 510 Fukuhara, A., Owaki, D., Kano, T., Kobayashi, R., and Ishiguro, A. (2018). Spontaneous gait transition to
511 high-speed galloping by reconciliation between body support and propulsion. *Advanced Robotics* 32,
512 794–808

- 513 Fukui, T., Fujisawa, H., Otaka, K., and Fukuoka, Y. (2019). Autonomous gait transition and galloping over
514 unperceived obstacles of a quadruped robot with cpg modulated by vestibular feedback. *Robotics and*
515 *Autonomous Systems* 111, 1–19
- 516 Grabowska, M., Godlewska, E., Schmidt, J., and Daun-Gruhn, S. (2012). Quadrupedal gaits in hexapod
517 animals – inter-leg coordination in free-walking adult stick insects. *Journal of Experimental Biology*
518 215, 4255–4266
- 519 Grillner, S. (1975). Locomotion in vertebrates: central mechanisms and reflex interaction. *Physiological*
520 *reviews* 55, 247–304
- 521 Grillner, S. (2003). The motor infrastructure: from ion channels to neuronal networks. *Nature Reviews*
522 *Neuroscience* 4, 573–586
- 523 Kimura, H., Fukuoka, Y., and Cohen, A. H. (2007). Adaptive dynamic walking of a quadruped robot
524 on natural ground based on biological concepts. *The International Journal of Robotics Research* 26,
525 475–490
- 526 Manoonpong, P., Parlitz, U., and Wörgötter, F. (2013). Neural control and adaptive neural forward models
527 for insect-like, energy-efficient, and adaptable locomotion of walking machines. *Frontiers in Neural*
528 *Circuits* 7, 12
- 529 Mantziaris, C., Bockemühl, T., Holmes, P., Borgmann, A., Daun, S., and Büschges, A. (2017). Intra-and
530 intersegmental influences among central pattern generating networks in the walking system of the stick
531 insect. *Journal of neurophysiology* 118, 2296–2310
- 532 Marder, E. and Bucher, D. (2001). Central pattern generators and the control of rhythmic movements.
533 *Current biology* 11, 986–996
- 534 Martin, L., Sándor, B., and Gros, C. (2016). Closed-loop robots driven by short-term synaptic plasticity:
535 Emergent explorative vs. limit-cycle locomotion. *Frontiers in neurorobotics* 10, 12
- 536 Miguel-Blanco, A. and Manoonpong, P. (2020). General distributed neural control and sensory adaptation
537 for self-organized locomotion and fast adaptation to damage of walking robots. *Frontiers in Neural*
538 *Circuits* 14, 46
- 539 Nomura, T., Kawa, K., Suzuki, Y., Nakanishi, M., and Yamasaki, T. (2009). Dynamic stability and phase
540 resetting during biped gait. *Chaos: An Interdisciplinary Journal of Nonlinear Science* 19, 026103
- 541 Owaki, D., Goda, M., Miyazawa, S., and Ishiguro, A. (2017). A minimal model describing hexapedal
542 interlimb coordination: the tegotae-based approach. *Frontiers in neurorobotics* 11, 29
- 543 Owaki, D. and Ishiguro, A. (2017). A quadruped robot exhibiting spontaneous gait transitions from walking
544 to trotting to galloping. *Scientific reports* 7, 1–10
- 545 Owaki, D., Kano, T., Nagasawa, K., Tero, A., and Ishiguro, A. (2013). Simple robot suggests physical
546 interlimb communication is essential for quadruped walking. *Journal of The Royal Society Interface* 10,
547 20120669
- 548 Pasemann, F., Hild, M., and Zahedi, K. (2003). So (2)-networks as neural oscillators. In *International*
549 *Work-Conference on Artificial Neural Networks* (Springer), 144–151
- 550 Rossignol, S., Dubuc, R., and Gossard, J.-P. (2006). Dynamic sensorimotor interactions in locomotion.
551 *Physiological reviews* 86, 89–154
- 552 Sándor, B., Jahn, T., Martin, L., and Gros, C. (2015). The sensorimotor loop as a dynamical system: how
553 regular motion primitives may emerge from self-organized limit cycles. *Frontiers in Robotics and AI* 2,
554 31
- 555 Sun, T., Shao, D., Dai, Z., and Manoonpong, P. (2018). Adaptive neural control for self-organized
556 locomotion and obstacle negotiation of quadruped robots. In *2018 27th IEEE International Symposium*
557 *on Robot and Human Interactive Communication (RO-MAN)* (IEEE), 1081–1086

- 558 Sun, T., Xiong, X., Dai, Z., and Manoonpong, P. (2020). Small-sized reconfigurable quadruped robot with
559 multiple sensory feedback for studying adaptive and versatile behaviors. *Frontiers in Neurorobotics* 14,
560 14
- 561 Taga, G., Yamaguchi, Y., and Shimizu, H. (1991). Self-organized control of bipedal locomotion by neural
562 oscillators in unpredictable environment. *Biological cybernetics* 65, 147–159
- 563 Tsujita, K., Tsuchiya, K., and Onat, A. (2001). Adaptive gait pattern control of a quadruped locomotion
564 robot. In *Proceedings 2001 IEEE/RSJ International Conference on Intelligent Robots and Systems.*
565 *Expanding the Societal Role of Robotics in the the Next Millennium (Cat. No. 01CH37180)* (IEEE),
566 vol. 4, 2318–2325